



# Anisotropic Flocking Control of Distributed Multi-Agent Systems using Fluid Abstraction

Matthew Silic\* and Zhuoyuan Song<sup>†</sup> and Kamran Mohseni<sup>‡</sup>  
*University of Florida, Gainesville, FL, 32611, USA*

**This paper presents a multi-agent flocking scheme for real-time control of homogeneous unmanned aerial vehicles (UAVs) based on smoothed particle hydrodynamics. Swarm cohesion, collision avoidance, and velocity consensus are concurrently satisfied by characterizing the emerging macroscopic flock as a continuous fluid. Two vital implementation issues are addressed in particular including latency in information fusion and directionality of communication due to antenna patterns. Symmetric control forces are achieved by meticulous scheduling of inter-vehicle communication to sustain the motion stability of the flock. A generalized, anisotropic smoothing kernel that takes into account the relative position and attitude between agents is adopted to address potential flocking instability introduced by communication anisotropy due to the antenna radiation pattern. The feasibility of the technique is demonstrated experimentally using a single UAV avoiding a virtual obstacle.**

## I. Introduction

The evolution of robotics does not cease as highly-intelligent, fully-autonomous platforms fulfill their missions independently at levels of sophistication that are comparable to or even superior to that of human individuals. Nature has exhibited the power of collaboration among individuals from the same species [1, 2], regardless of their habitats, trophic levels or stimulus, in predator evasion [3], foraging [4], migration [5], or magnification of social impact [6]; (see Fig. 1). Although far from their ultimate maturity, existing mobile robots of almost all kinds, from micro-robots [7] to underwater vehicles [8], have been exploited to explore and reproduce the fascinating motion by those biological swarms. More importantly, robotic networks in collaboration have shown undeniable advantages over individual platforms in expanding the coverage of the robots, improving remote sensing efficiency, and accomplishing tasks that are otherwise impossible for a single robot [9].

Although existing studies have achieved some success in the control of multi-robot network systems [10–14], the presence of strong geophysical flows (Fig. 2) significantly complicates the problem. Robotic sensor nodes such as micro aerial vehicles (MAVs) and autonomous underwater vehicles (AUVs) are often relatively small in size and limited in actuation compared to their conventional counterparts in order to maintain cost-effective designs. Unfortunately, this leaves them susceptible to strong environmental forces resulted from the background flows. These geophysical flows often act as a dominating factor in sensor node mobility; therefore they can no longer be loosely treated as disturbances. To this end, several recent studies have been focusing on the control and path planning of mobile robots in known background flows [15–19]. However they either fail to address the complex intra-network interactions in background flows or tackle merely agent-flow interactions, which do not reveal the macroscopic network motion under the impact of the background flows.

Considering the recent progress in geophysical flow modeling, we believe that it is the time to start treating the mobile sensor network and the underlying geophysical flow as a single integrated dynamical system. Due to the relatively small sizes of the mobile agents of interest, it is reasonable to first consider the one-way coupling relationship between the flow sub-system and the network sub-system, i.e. the sensor network motion does not alter the background flow dynamics. The macroscopic dynamics of the sensor network as an emergent continuum is the critical link that bridges the background flow dynamics and the local intra-network interactions. Two major sectors of this research are: (1) understanding the emergent sensor network dynamics as a component that constitutes the integrated network-flow dynamical system, and (2) controlling the behavior of the integrated network-flow dynamical system through altering the sensor network configuration. To this end, it is crucial to develop a cooperative control algorithm for mobile robot

\*Graduate research assistant, Department of Mechanical and Aerospace Engineering.

<sup>†</sup>Graduate research assistant, Department of Mechanical and Aerospace Engineering.

<sup>‡</sup>William P. Bushnell Endowed Professor of Mechanical and Aerospace Engineering Department and Electrical and Computer Engineering Department, Institute for Networked Autonomous Systems. AIAA associate fellow.



**Fig. 1** (a) A school of smaller fish keeping their distance when a blacktip reef shark swims amongst them in shallow water in the Maldives (Photograph by Paul Wilkinson); (b) A flock of blue-footed Booby (*Sula nebouxii*) flock diving for fish around Galapagos Islands (Photograph by Winfried Wisniewski); (c) A sea of red crabs marching down the road on Christmas Island in the Indian Ocean come to a standstill, as their annual mating season gets underway (Photograph by Gary Tindale); (d) A Mexican wave at an American football game (taken from [6]).



**Fig. 2** Left: Hurricane Isabel. (Credit: Earth Sciences & Image Analysis Laboratory, Johnson Space Center.) Right: General ocean circulation. (Credit: NASA/Goddard Space Flight Center Scientific Visualization Studio.)

networks that allows emerging macroscopic dynamics resembling the underlying environment while facilitating the control of preferable flocking behavior.

## II. Abstraction in Swarm Robotics

Many techniques have been introduced in the past for vehicle swarm control include flocking, formation control, and hierarchical cooperation control [14, 20, 21]. With few exceptions [18, 22, 23], these techniques do not account for large background flows. Previously, we proposed a multi-vehicle control algorithm that combines both flocking control and flock guidance [24]. Vehicles are treated as fluid particles under this control scheme. Fundamental conservation laws governing fluid motion are applied to the vehicle fleet through smoothed particle hydrodynamics (SPH) [25], ensuring flock cohesion and collision avoidance by satisfying the underlying conservation laws. Macroscopic fluid properties are assigned to vehicles through local smoothing, resulting in a fully distributed control law.

## III. Smoothed Particle Hydrodynamics

A complete description of fluid dynamics includes the conservation of mass, momentum, and energy, and an *equation of state* that relates density, temperature and pressure. For inviscid fluids, the relevant equations are the Euler equations:

$$\frac{\partial \rho}{\partial t} + \nabla \cdot (\rho \mathbf{v}) = 0, \quad (1)$$

$$\frac{\partial}{\partial t}(\rho \mathbf{v}) + \nabla \cdot (\mathbf{v} \times (\rho \mathbf{v})) + \nabla P + F_{ext} = 0. \quad (2)$$

Here,  $\rho$  is density,  $\mathbf{v}$  is fluid velocity,  $P$  is pressure,  $F_{ext}$  is any external force, and  $t$  is time. Typically, an equation of state relating the fluid density to pressure is also needed. These partial differential equations represent the fluid as a continuum with an infinite number of degrees of freedom. SPH discretizes continuous fluid properties into individual

particles through *smoothing kernel* functions  $W(\mathbf{r}_{ij}, h)$ , where  $h$  is the smoothing width of the kernel, and  $\mathbf{r}_{ij} = \mathbf{r}_i - \mathbf{r}_j$  is the relative position vector between particles  $i$  and  $j$ . Such an approximation scheme is known to have second-order accuracy or  $h^2$  accuracy [25, 26]. Under such a discretization scheme, the particle density equation and the conservation of momentum can be derived from the Navier-Stokes equations as

$$\rho_i = \sum_j W(\mathbf{r}_{ij}, h) m_j, \quad (3)$$

$$\begin{aligned} \frac{d\mathbf{v}_i}{dt} = & - \sum_j m_j \left( \frac{P_i}{\rho_i^2} + \frac{P_j}{\rho_j^2} \right) \nabla_i W(\mathbf{r}_{ij}, h) \\ & + \sum_j m_j \frac{2\mu}{\rho_i \rho_j} \frac{\mathbf{v}_{ij}}{\|\mathbf{r}_{ij}\|} \frac{dW_{ij}}{d\|\mathbf{r}_{ij}\|}, \end{aligned} \quad (4)$$

for mass  $m$  and viscosity coefficient  $\mu$ . The velocity vector is the time derivative of the position vector  $\mathbf{v}_i = \dot{\mathbf{r}}_i$ . The operator  $\nabla_i$  represents the gradient with respect to the coordinates of particle  $i$ , and the relative velocity between two different particles is  $\mathbf{v}_{ij} = \mathbf{v}_i - \mathbf{v}_j$ . The SPH algorithm allows controlling heterogeneous vehicle swarms under the same control scheme. Different fluid properties and behavior can be achieved through adjusting individual vehicle properties such as smoothing length and particle mass, which allows us to introduce a reduced density particle to create a low-pressure region that generates attractive forces for the purpose of flock guidance.

To the best of our knowledge, the first implementation of SPH in robotic swarm control was reported by [27], who studied a sensor coverage problem with obstacle avoidance using SPH to generate local control for a robot swarm. Later, [28] developed a two-level robot swarm control scheme using SPH to accomplish missions including robot swarm deployment, dispatching, and flocking. Many other previous works have also used SPH in a cooperative control context for different applications with generally good results [24, 29–33]. In many ways, SPH control is similar to control using artificial potential fields. However, since SPH provides a complete description of fluid dynamics, it includes more properties that are beneficial to multi-vehicle control problems. For instance, SPH includes viscous forces that provide velocity consensus effect, which would need to be added to other artificial potential based control schemes. Additionally, with similar force-distance potentials, the density variable in the SPH-based control scheme provides more consistent inter-vehicle spacing control than artificial potential based control schemes.

## IV. Implementation Consideration

The distributed nature of SPH makes it well-suited for practical implementations with real-time robotic systems. However, deliberation is typically required before real-world implementation of a cooperative control algorithm in order to account for the physical limitations of a robotic system. In this paper, we focus on addressing two implementation issues that prevents generic SPH algorithm from being applied to a multi-UAV network. Firstly, a scheduling scheme is designed to address the latency within inter-agent communication. Secondly, a generalized smoothing kernel function for approximating SPH quantities is adopted to tackle the directivity constraint of inter-agent communication resulted from the 3D dipole antenna pattern. It is known that the force calculation must be symmetric in agent- $i$  and agent- $j$  in order to ensure that momentum is globally conserved [34]. Therefore, the proposed solutions to both issues guarantee symmetry of SPH forces generation by interacting agents.

### A. Communication Latency

We focus on the case where all  $N$  agents are synchronized and inter-agent communication is through schedule broadcasting where only one agent is scheduled to broadcast its data packet to its reachable neighbors. At the end of each broadcast cycle, a *silence period* is allocated for all agents to computed virtual interaction forces based on the SPH formulation. Figure 3 briefly illustrates the communication scheduling scheme where  $t_i$  indicates the time stamp when the packet being broadcast by agent- $i$  is generated. The span between consecutive time stamps are allocated to be sufficiently large to accommodate the transmission of the data packet.

To enforce symmetry of the virtual interaction force, each agent uses approximated ego-state and neighbor-state during SPH computation. We denote the data packet broadcast by agent- $i$  at time  $t_i$  as  $\mathbf{P}_{t_i} \equiv [\rho_{t_i}, \mathbf{r}_i^{t_i}, \mathbf{v}_i^{t_i}, \dot{\mathbf{v}}_i^{t_i}]$ . Assuming that the change in local flock density is negligible within one communication cycle, i.e.  $\hat{\rho}_i^{t_{\text{sp}}} \approx \rho_i^{t_i} \forall i = 1, \dots, N$ , agent- $i$  performs dead-reckoning for its ego-state from  $t_i$  and for its neighbor  $j$ 's state from  $t_j$  assuming the

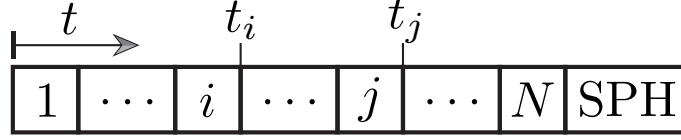


**Fig. 3 Illustration of broadcasting schedule proposed for ensuring symmetric interaction control decision.**

acceleration remains constant during dead-reckoning:

$$\hat{\mathbf{v}}_i^{i \rightsquigarrow \text{sph}} = \mathbf{v}_i^{t_i} + \dot{\mathbf{v}}_i^{t_i} \cdot \Delta t_i^{\text{sph}}, \quad (5)$$

$$\hat{\mathbf{r}}_i^{i \rightsquigarrow \text{sph}} = \mathbf{r}_i^{t_i} + \mathbf{v}_i^{t_i} \cdot \Delta t_i^{\text{sph}} + \frac{1}{2} \cdot \dot{\mathbf{v}}_i^{t_i} \cdot (\Delta t_i^{\text{sph}})^2, \quad (6)$$

where the superscript “ $i \rightsquigarrow \text{sph}$ ” indicates dead-reckoning quantities from  $t_i$  to  $t_{\text{sph}}$  and will be omitted for the rest of the paper. The SPH control law (4) for agent- $i$  at  $t_{\text{sph}}$  can be rewritten as

$$\begin{aligned} \dot{\mathbf{v}}_i^{t_{\text{sph}}} = & - \sum_{j=1}^N m_j \left( \frac{\hat{p}_i}{\hat{\rho}_i^2} + \frac{\hat{p}_j}{\hat{\rho}_j^2} \right) \nabla_i W(\hat{\mathbf{r}}_{ij}, h) \\ & + \sum_j m_j \frac{2\mu}{\hat{\rho}_i \hat{\rho}_j} \frac{\hat{\mathbf{v}}_{ij}}{\|\hat{\mathbf{r}}_{ij}\|} \frac{dW_{ij}}{d\|\hat{\mathbf{r}}_{ij}\|}, \end{aligned} \quad (7)$$

where pressure can be computed based on the corresponding density as  $\hat{P}_i = B[\hat{\rho}_i/\rho_0 - 1]$  with  $B$  the bulk number and  $\rho_0$  being the natural density.

All information used in (7) is shared between agent- $i$  and its interacting neighbor  $j$ . Therefore, virtual interaction forces computed independently by agent- $i$  and agent- $j$  are symmetric, i.e.  $\hat{\mathbf{v}}_{ij}^{t_{\text{sph}}} = \hat{\mathbf{v}}_{ji}^{t_{\text{sph}}}$ . It has been pointed out by Shapiro et al. [34] that this is a vital criterion to ensure the conservation of momentum of the macroscopic fluidic behavior. It also helps preserve the stability characteristics of the agent network from a control perspective since previous studies on swarm stability of a SPH-controlled swarm depends heavily on symmetry in interactions.

It is worth mentioning that the control law (7) is not an exact implementation of the SPH formulation given the actual states of the agent network. Instead, it is an approximated realization the accuracy of which depends on the duration of a scheduled communication cycle. For applications with aerial vehicles where inter-agent communication are through radio frequency, we expect the approximation error to be negligible. For agent networks with large communication delays such as underwater applications, further investigation is required justify the validity of this scheduling scheme. Potential adversary effect due to packet loss is also not considered here and will be addressed individually in a future effort.

## B. Communication directivity

Similar to many existing cooperative control algorithms, the SPH-based flocking law does not consider the potential communication directivity by applying an isotropic smoothing kernel function, the most popular form of which is the cubic spline devised by Monaghan and Lattanzio [35]

$$W(\mathbf{r}_{ij}, h) = \frac{C}{h^d} \begin{cases} 4 - 6s^2 + 3s^3 & \text{if } 0 \leq s \leq 1 \\ (2 - s)^3 & \text{if } 1 < s \leq 2 \\ 0 & \text{if } s > 2 \end{cases}, \quad (8)$$

where  $d$  is the dimension of the problem,  $h$  is the smoothing width,  $s = \|\mathbf{r}_{ij}\|/h$ , and  $C$  is the normalizing coefficient that takes the value of  $1/6$ ,  $5/(14\pi)$ , and  $1/(4\pi)$  for  $d = 1, 2, 3$ , respectively. In the case of  $d = 3$ , the smoothing kernel shapes as a sphere, defining the *region of impact* (RoI) of the corresponding agent on its neighbors.

In practice, however, the RoI is dictated by the range of communication. For aerial vehicles using radio frequency for communication, the range of communication often shows strong directivity due to the antenna radiation pattern [36]. The radiation pattern for a dipole antenna can be characterized by the normalized radiation pattern

$$E(\theta) = \left| \frac{\cos(\frac{\pi L}{\lambda} \cos \theta) - \cos(\frac{\pi L}{\lambda})}{\sin \theta} \right|^2, \quad (9)$$

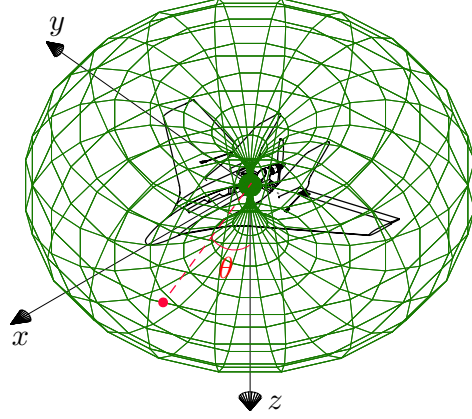


**Fig. 4** Coordinate system defining used to define the radiation pattern of an antenna. Along the axis of the antenna (i.e. the  $z$ -axis), the gain has a null value.

where  $L$  is the length of the antenna,  $\lambda$  is the radio signal wavelength, and  $\theta$  is the polar angle (see Figure 4). The RoI of a uniaxial antenna can be approximated by the three-dimensional radiation pattern of a half-wave dipole. Due to the directivity of RF communication with a dipole antenna, simply defining the RoI as an isotropic sphere will lead to potential issue when agents appear in the RoI of on another but cannot exchange information given their relative attitude.

To account for the anisotropy of inter-agent communication and define an attitude-aware RoI for each agent, a generalized three-dimensional smoothing kernel function is adopted such that the approximation of continuous fluid quantities depends not only on the relative distance between interacting agents but also on their attitude. Such a generalization was inspired by the anisotropic smoothing kernel first used by Shapiro [37, 38] for cosmological gas dynamics, where a one-dimensional, planar, cosmological pancake collapse was simulated with a three-dimensional, SPH code. The SPH formulation with anisotropic smoothing kernel was often named adaptive SPH (ASPH) for it allowing the smoothing kernel to be dynamically evolving during numerical simulation.

The anisotropic smoothing scheme starts with a linear transformation  $G : \mathbf{r} \mapsto \boldsymbol{\eta}$  such that  $\boldsymbol{\eta} = G\mathbf{r}$ , where  $\mathbf{r}$  is the position vector of the agent and  $\boldsymbol{\eta}$  can be considered as the normalized position vector [39]. The linear transformation is a function of smoothing length and dictates the anisotropy of the RoI. Denoting the earth-fixed frame as  $\{n\}$  and the body-fixed frame of an agent as  $\{b\}$ , the transformation matrix in the body frame is  $G^{(b)} = \text{diag}(h_1, h_2, h_3)$  in three-dimensional case. Here  $h_i$  dictates the range of RoI along each principal axis of the vehicle's body-fixed coordinates. The 3D RoI becomes an ellipsoid when  $h_i$  are not equivalent (anisotropic) and a sphere otherwise (isotropic). In practice, the values of  $h_i$  can be properly chosen to reflect the antenna radiation pattern. Given the Euler angles ( $\phi, \theta, \psi$ ) of the vehicle, the transformation matrix in the inertial frame can be easily computed as

$$G \equiv G^{(n)} = R_b^n \cdot G^{(b)} \cdot (R_b^n)^\top, \quad (10)$$

where  $R_b^n \in SO(3)$  is the rotational matrix determined by the Euler angles.

Implementing the generalized kernel function merely requires replacing the original isotropic kernel  $W(\mathbf{r}, h)$  with  $W(\boldsymbol{\eta})$ . Similarly, a feasible form of the generalized kernel function can be

$$W(\boldsymbol{\eta}) = \frac{\det(G)}{4\pi} \begin{cases} 4 - 6\|\boldsymbol{\eta}\|^2 + 3\|\boldsymbol{\eta}\|^3 & \text{if } 0 \leq \|\boldsymbol{\eta}\| \leq 1 \\ (2 - \|\boldsymbol{\eta}\|)^3 & \text{if } 1 < \|\boldsymbol{\eta}\| \leq 2 \\ 0 & \text{if } \|\boldsymbol{\eta}\| > 2 \end{cases}. \quad (11)$$

One complexity introduced by this generalization appears when computing its gradient, which is required by the SPH



**Fig. 5** Left: The delta wing flock on display. Right: Close-up on the autopilot embarked on the delta wing.

calculation. Based on the chain rule, one can find

$$\nabla W(\boldsymbol{\eta}) = G \frac{\partial W}{\partial \boldsymbol{\eta}} + \mathbf{r} \frac{\partial G}{\partial \mathbf{r}} \frac{\partial W}{\partial \boldsymbol{\eta}} \stackrel{0}{\approx} G \frac{\boldsymbol{\eta}}{\|\boldsymbol{\eta}\|} \frac{\partial W}{\partial \|\boldsymbol{\eta}\|}. \quad (12)$$

In the case where the antenna radiation is independent from the position of the vehicle, which is generally the case, the second term of (12) goes to zero. Then the gradient of kernel function (11) can be calculated as

$$\nabla W(\boldsymbol{\eta}) = \det(G) G \cdot \frac{1}{4\pi} \frac{\boldsymbol{\eta}}{\|\boldsymbol{\eta}\|} \begin{cases} 4 - 6\|\boldsymbol{\eta}\|^2 + 3\|\boldsymbol{\eta}\|^3 & \text{if } 0 \leq \|\boldsymbol{\eta}\| \leq 1 \\ (2 - \|\boldsymbol{\eta}\|)^3 & \text{if } 1 < \|\boldsymbol{\eta}\| \leq 2 \\ 0 & \text{if } \|\boldsymbol{\eta}\| > 2 \end{cases}. \quad (13)$$

Another complexity brought by the anisotropic kernel function is its dependency on the agent's attitude. To guarantee the symmetry of SPH interaction among agents, two extra steps are required. Firstly, the data packet transmitted among agents is augmented to include the Euler angles. Secondly, a symmetrization step is required for interacting agent pairs since they possess kernel functions with different coefficients, which are functions of their own Euler angle. This can be accomplished utilizing the symmetrization scheme introduced by Hernquist and Katz [40] such that

$$W_{ij} = \frac{1}{2} [W(\boldsymbol{\eta}_i) + W(\boldsymbol{\eta}_j)], \quad (14)$$

where  $\boldsymbol{\eta}_i \equiv G_i \mathbf{r}_{ij}$  and  $\boldsymbol{\eta}_j \equiv G_j \mathbf{r}_{ji}$ .

## V. Field Deployment

The experimental platform used to demonstrate the feasibility of the SPH control algorithm is described in this section. A complete description of the system can be found in [41]. Following the description of the system, the results from the field deployment are presented.

The platform used in the experimental validation is shown in Fig. 5, left. The aircraft has a wingspan of 37 inches and weighs less than 0.5 kg. The UAV is equipped with the AMP custom autopilot [42]. The autopilot (Fig. 5, right) is a collection of electronic devices, namely a GPS receiver, a radio transceiver, a barometer, an atmospheric sensor and an MARG sensor. A MARG sensor is a single IC that houses a magnetometer, an accelerometer, and a rate gyro. Additionally, an Xbee wireless radio can plug into headers on the underside of the autopilot board; the Xbee is used to transmit and receive information. The autopilot controls the horizontal position of the aircraft by varying the roll angles. Pitch and throttle are varied in order to control the altitude. The autopilot system also includes a complementary groundstation which is comprised of a laptop and an Xbee radio.

UAV guidance is effected through a combination of two schemes: vector field guidance and SPH guidance. Let  $\vec{q}_{\text{field}}$  represent the guidance vector from the vector field and let  $\vec{a}_{\text{SPH}}$  represent the acceleration due to the SPH force. To obtain the total guidance vector, the guidance vector from the vector field is normalized and added to a scaled version of the SPH acceleration vector:

$$\vec{q}_{\text{tot}} = \beta \vec{a}_{\text{SPH}} + \frac{\vec{q}_{\text{field}}}{\|\vec{q}_{\text{field}}\|}. \quad (15)$$

The scaling factor  $\beta$  allows us to control the relative strength of the two guidance schemes. For the test presented herein,  $\beta$  is set to 0.2.

For this test, the vector field is used to guide the UAV to a loiter circle with a radius of 100 meters. A virtual obstacle is placed on the eastward side of the loiter circle. The smoothing width of the obstacle is 40 meters. When the vehicle is outside the domain of influence of the obstacle, the SPH acceleration is zero and the UAV is guided solely by the vector field. However, when the UAV enters the domain of influence of the obstacle, the resulting SPH pressure force repels the vehicle, pushing it off the loiter circle. The ground track from this experiment is shown in Fig. 6.

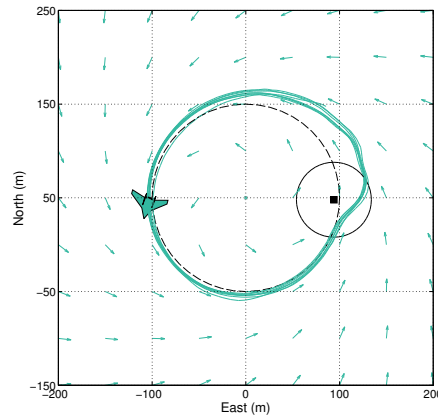


**Fig. 6** Single vehicle avoiding a virtual obstacle. The vector field is used to guide the UAV to the loiter circle, represented by the black dashed line. The black solid line denotes the domain of influence of the obstacle.

## VI. Conclusion

This paper presents a multi-agent flocking scheme for real-time control of homogeneous unmanned aerial vehicles (UAVs) based on smoothed particle hydrodynamics. We address two implementation issues that prevents the generic SPH algorithm from being applied to a multi-UAV network. Firstly, we develop a scheduling scheme designed to address the latency within inter-agent communication. Secondly, we propose a generalized smoothing kernel function for approximating SPH quantities in order to tackle the directivity constraint of inter-agent communication resulted from the 3D dipole antenna pattern. We successfully implement the SPH based controller on an autonomous UAV with limited processing capabilities.

## References

- [1] Parrish, J., and Edelstein-Keshet, L., "Complexity, pattern, and evolutionary trade-offs in animal aggregation," *Science*, Vol. 284, No. 5411, 1999, pp. 99–101. doi:10.1126/science.284.5411.99, URL <http://science.sciencemag.org/content/284/5411/99>.
- [2] Sumpter, D., "The principles of collective animal behaviour," *Philosophical Transactions of the Royal Society of London B: Biological Sciences*, Vol. 361, No. 1465, 2006, pp. 5–22. doi:10.1098/rstb.2005.1733, URL <http://rstb.royalsocietypublishing.org/content/361/1465/5>.
- [3] Olson, R., Hintze, A., Dyer, F., Knoester, D., and Adami, C., "Predator confusion is sufficient to evolve swarming behaviour," *Journal of the Royal Society Interface*, Vol. 10, No. 85, 2013, p. 20130305. doi:10.1098/rsif.2013.0305, URL <http://www.ncbi.nlm.nih.gov/pmc/articles/PMC4043163/>.
- [4] Carroll, C., and Janzen, D., "Ecology of foraging by ants." *Annual Review of Ecology and Systematics*, Vol. 4, 1973, pp. 231–257. URL <http://www.jstor.org/stable/2096812>.

- [5] Collett, M., Despland, E., Simpson, S., and Krakauer, D., "Spatial scales of desert locust gregarization," *Proceedings of the National Academy of Sciences of the United States of America*, Vol. 95, No. 22, 1998, pp. 13052–13055. URL <http://www.ncbi.nlm.nih.gov/pmc/articles/PMC23706/>.
- [6] Farkas, I., Helbing, D., and Vicsek, T., "Social behaviour: Mexican waves in an excitable medium," *Nature*, Vol. 419, No. 6903, 2002, pp. 131–132. doi:10.1038/419131a, URL <http://dx.doi.org/10.1038/419131a>.
- [7] Rubenstein, M., Cornejo, A., and Nagpal, R., "Programmable self-assembly in a thousand-robot swarm," *Science*, Vol. 345, No. 6198, 2014, pp. 795–799. doi:10.1126/science.1254295.
- [8] Zahadat, P., Hahshold, S., Thenius, R., Crailsheim, K., and Schmickl, T., "From honeybees to robots and back: Division of labour based on partitioning social inhibition," *Bioinspiration & Biomimetics*, Vol. 10, No. 6, 2015, p. 066005. URL <http://stacks.iop.org/1748-3190/10/i=6/a=066005>.
- [9] Şahin, E., *Swarm robotics: From sources of inspiration to domains of application*, Springer Berlin Heidelberg, Berlin, Heidelberg, 2005, pp. 10–20. doi:10.1007/978-3-540-30552-1\_2.
- [10] Leonard, N., and Fiorelli, E., "Virtual leaders, artificial potentials and coordinated control of groups," *Proceedings of the IEEE Conference on Decision and Control (CDC)*, Vol. 3, Orlando, FL, USA, 2001, pp. 2968–2973. doi:10.1109/2001.980728.
- [11] Jadbabaie, A., Lin, J., and Morse, A. S., "Coordination of groups of mobile autonomous agents using nearest neighbor rules," *IEEE Transactions on Automatic Control*, Vol. 48, No. 6, 2003, pp. 988–1001. doi:10.1109/TAC.2003.812781, URL <http://dx.doi.org/10.1109/TAC.2003.812781>.
- [12] Olfati-Saber, R., "Flocking for multi-agent dynamic systems: Algorithms and theory," *IEEE Transactions on Automatic Control*, Vol. 51, No. 3, 2006, pp. 401–420. doi:10.1109/TAC.2005.864190, URL <http://dx.doi.org/10.1109/TAC.2005.864190>.
- [13] Murray, R. M., "Recent research in cooperative control of multivehicle systems," *Journal of Dynamic Systems, Measurement, and Control*, Vol. 129, No. 5, 2007, pp. 571–583. doi:10.1115/1.2766721, URL <http://dx.doi.org/10.1115/1.2766721>.
- [14] Brambilla, M., Ferrante, E., Birattari, M., and Dorigo, M., "Swarm robotics: A review from the swarm engineering perspective," *Swarm Intelligence*, Vol. 7, No. 1, 2013. doi:10.1007/s11721-012-0075-2.
- [15] Inanc, T., Shadden, S., and Marsden, J., "Optimal trajectory generation in ocean flows," *Proceedings of the American Control Conference (ACC)*, Portland, OR, USA, 2005, pp. 674–679.
- [16] Paley, D. A., and Peterson, C., "Stabilization of collective motion in a time-invariant flowfield," *Journal of Guidance, Control, and Dynamics*, Vol. 32, No. 3, 2009, pp. 771–779.
- [17] Lolla, T., Ueckermann, M. P., Yigit, K., Haley, P. J., and Lermusiaux, P. F. J., "Path planning in time dependent flow fields using level set methods," *Proceedings of the IEEE International Conference on Robotics and Automation (ICRA)*, St. Paul, MN, USA, 2012, pp. 166–173.
- [18] DeVries, L., and Paley, D., "Multi-vehicle Control in a Strong Flowfield with Application to Hurricane Sampling," *Journal of Guidance, Control, and Dynamics*, Vol. 35, No. 3, 2012. doi:10.2514/1.55580.
- [19] Mallory, K., Hsieh, M. A., Forgoston, E., and Schwartz, I. B., "Distributed allocation of mobile sensing swarms in gyre flows," *Nonlinear Processes in Geophysics*, Vol. 20, No. 5, 2013, pp. 657–668. doi:10.5194/npg-20-657-2013.
- [20] Barca, J. C., and Sekercioglu, Y. A., "Swarm robotics reviewed," *Robotica*, Vol. 31, 2013, pp. 345–359. doi:10.1017/S026357471200032X.
- [21] Ren, W., Beard, R. W., and Atkins, E. M., "A survey of consensus problems in multi-agent coordination," *Proceedings of the American Control Conference*, IEEE, 2005, pp. 1859–1864.
- [22] Lipinski, D., and Mohseni, K., "A master-slave fluid cooperative control algorithm For optimal trajectory planning," *Proceedings of the IEEE International Conference on Robotics and Automation (ICRA)*, Shanghai, China, 2011, pp. 3347–3351. doi:10.1109/ICRA.2011.5980401, URL <http://dx.doi.org/10.1109/ICRA.2011.5980401>.
- [23] Song, Z., Lipinski, D., and Mohseni, K., "Multi-vehicle cooperation and nearly fuel-optimal flock guidance in strong background flows," *Ocean Eng.*, Vol. 141, 2017, pp. 388–404. doi:10.1016/j.oceaneng.2017.06.024, URL <http://www.sciencedirect.com/science/article/pii/S0029801817303189>.

- [24] Shaw, A., and Mohseni, K., "A fluid dynamic based coordination of a wireless sensor network of unmanned aerial vehicles: 3-D simulation and wireless communication characterization," *IEEE Sensors Journal, Special Issue on Cognitive Sensor Networks*, Vol. 11, No. 3, 2011, pp. 722–736. doi:10.1109/JSEN.2010.2064294, URL <http://dx.doi.org/10.1109/JSEN.2010.2064294>.
- [25] Monaghan, J. J., "Smoothed particle hydrodynamics," *Annual Review of Astronomy and Astrophysics*, Vol. 30, 1992, pp. 543–574. doi:10.1146/annurev.aa.30.090192.002551, URL <http://dx.doi.org/10.1146/annurev.aa.30.090192.002551>.
- [26] Liu, G. R., and Liu, M. B., *Smoothed Particle Hydrodynamics: A Meshfree Particle Method*, World Scientific, Hackensack, NJ, USA, 2003.
- [27] Perkinson, J. R., and Shafai, B., "A Decentralized Control Algorithm for Scalable Robotic Swarms Based on Mesh-Free Particle Hydrodynamics," *Proceedings of the IASTED International Conference on Robotics and Applications*, Cambridge, MA, USA, 2005, pp. 1–6.
- [28] Pac, M., Erkmén, A., and Erkmén, I., "Control of robotic swarm behaviors based on smoothed particle hydrodynamics," *Proceedings of the IEEE/RSJ International Conference on Intelligent Robots and Systems (IROS)*, San Diego, CA, USA, 2007, pp. 4194–4200. doi:10.1109/IROS.2007.4399437.
- [29] Huhn, S., and Mohseni, K., "Cooperative control of a team of AUVs using smoothed particle hydrodynamics with restricted communication," *Proceedings of the ASME International Conference on Ocean, Offshore and Arctic Engineering*, Honolulu, HI, USA, 2009, pp. 531–538. doi:10.1115/OMAE2009-79869, URL <http://dx.doi.org/10.1115/OMAE2009-79869>.
- [30] Lipinski, D., and Mohseni, K., "Cooperative control of a team of unmanned vehicles using smoothed particle hydrodynamics," *Proceedings of the AIAA Guidance, Navigation, and Control Conference*, Toronto, Canada, 2010. doi:10.2514/6.2010-8316, URL <http://dx.doi.org/10.2514/6.2010-8316>.
- [31] Pimenta, L. C. A., Michael, N., Mesquita, R. C., Pereira, G. A. S., and Kumar, V., "Control of swarms based on Hydrodynamic models," *Proceedings of the IEEE International Conference on Robotics and Automation (ICRA)*, Pasadena, CA, USA, 2008, pp. 1948–1953. doi:10.1109/ROBOT.2008.4543492.
- [32] Pimenta, L. C. A., Pereira, G. A. S., Michael, N., Mesquita, R. C., Bosque, M. M., Chaimowicz, L., and Kumar, V., "Swarm Coordination Based on Smoothed Particle Hydrodynamics Technique," *IEEE Transactions on Robotics*, Vol. 29, No. 2, 2013, pp. 383–399. doi:10.1109/TRO.2012.2234294.
- [33] Zhao, S., Ramakrishnan, S., and Kumar, M., "Density-based control of multiple robots," *Proceedings of the American Control Conference (ACC)*, San Francisco, CA, USA, 2011, pp. 481–486.
- [34] Shapiro, P. R., Martel, H., Villumsen, J. V., and Owen, J. M., "Adaptive smoothed particle hydrodynamics, with application to cosmology: Methodology," *Astrophysical Journal Supplement*, Vol. 103, 1996, pp. 269–330. doi:10.1086/192279, URL <http://adsabs.harvard.edu/abs/1996ApJS...103..269S>.
- [35] Monaghan, J., and Lattanzio, J., "A refined particle method for astrophysical problems," *Astron. Astrophys.*, Vol. 149, 1985, pp. 135–143.
- [36] Stutzman, W., and Thiele, G., *Antenna Theory and Design*, Antenna Theory and Design, Wiley, 2012.
- [37] Shapiro, P., "The intergalactic medium and galaxy formation," *Annals of the New York Academy of Sciences*, Vol. 571, No. 1, 1989, pp. 128–150. doi:10.1111/j.1749-6632.1989.tb50502.x, URL <http://dx.doi.org/10.1111/j.1749-6632.1989.tb50502.x>.
- [38] Shapiro, P., Kang, H., and Villumsen, J., "A new method for three-dimensional hydrodynamical  $N$ -body simulations of large-scale cosmological flows," *Large-scale Structures and Peculiar Motions in the Universe*, Astronomical Society of the Pacific Conference Series, Vol. 15, edited by D. Latham and L. da Costa, 1991, p. 119.
- [39] Owen, J., Villumsen, J., Shapiro, P., and Martel, H., "Adaptive smoothed particle hydrodynamics: Methodology. II." *The Astrophysical Journal Supplement Series*, Vol. 116, No. 2, 1998, p. 155. URL <http://stacks.iop.org/0067-0049/116/i=2/a=155>.
- [40] Hernquist, L., and Katz, N., "TREESPH - A unification of SPH with the hierarchical tree method," *The Astrophysical Journal Supplement Series*, Vol. 70, 1989, pp. 419–446. doi:10.1086/191344.
- [41] Hodgkinson, B., Lipinski, D., Peng, L., and Mohseni, K., "High resolution atmospheric sensing using UAV swarms," *Proceedings of the International Symposium on Distributed Autonomous Robotic Systems*, Daejeon, South Korea, 2014, pp. 31–45. doi:10.1007/978-3-642-55146-8, URL <http://dx.doi.org/10.1007/978-3-642-55146-8>.

- [42] Binger, A., and Mohseni, K., “AMP: Lightweight, Low-Resource Autopilot System for Micro/Miniature Mobile Sensing Platforms,” *AIAA Journal Aerospace Information Systems*, 2017.